

Spin inversion devices with Fano anti-resonances

J. L. Cardoso and P. Pereyra

*Física Teórica y Materia Condensada, UAM-Azcapotzalco,
Avenida San Pablo 180, Código Postal 02200 México Distrito Federal, México*

(Dated: February 16, 2022)

Analyzing spin transport of quasi-2D electrons g moving through a semiconductor wave guide subject to a sectionally homogeneous tilted magnetic field, we found well-defined selection rules for resonant and antiresonant spin carrier transmission. Based on these selection rules and the band shift induced by the magnetic field strength and the tilting angles, we propose an efficient spin inversion device. For a polarized incoming electron beam, we can determine from our theoretical approach, physical conditions for spin-inversion efficiency up to 80%. We visualize this mechanism in terms of conductance and the spacial behavior of the wave function amplitude along the superlattice.

PACS numbers: 03.65.Nk 75.10.Jm

The design of simple and efficient devices working as reliable sources of spin-polarized electrons¹ is one of the main goals in the spintronics field. It has been partially achieved with different degrees of efficiency, confidence and accuracy, both experimentally and theoretically. On the experimental side, spin injection devices into semiconductor structures have evolved from ferromagnetic metallic contacts^{2,3} and diluted magnetic semiconductor spin-aligner structures^{4,5,6,7,8}, to optical systems sensitive to spin orientation^{9,10,11}. On the theoretical side, the spin carriers transport problem spurred an intense research activity where a large number of different approaches and systems were studied, from open quantum dots^{12,13} to magnetic superlattices^{14,15}. Concerning the control of spin-carriers currents, one of the relevant problems is the manipulation at will of the spin orientation, i.e. the ability to invert whenever it is necessary the carriers spin orientation. In this letter we discuss physical conditions for an efficient spin-inversor device. Among the numerous spin-filter devices proposed in the literature, it was shown that the homogeneous magnetic superlattice (HMS) can, in principle, work as a 100% spin-polarizer¹⁴ and as a simple system to induce spin-flipping processes when the external magnetic field is tilted¹⁶. These processes, visualized through the spatial evolution of the spin-carrier wave functions¹⁶, lead us to suggest here physical conditions for a simple and highly efficient two-step spin-inversor device, with a HMS of length L for each step.

If we have a quasi-2D semiconductor waveguide of length $L_S > 2L$ and transversal widths w_y and w_z (with $w_z \ll w_y$), one can produce two consecutive superlattices of length L , without growing layers of different type of materials, by coating alternating stripes of length L_F of the semiconductor with some field-screening material¹⁸. Thus, an external magnetic field \vec{H} , acts only on the uncoated stripes of length L_H and a magnetic superlattice $FHFHFHF \dots$ is formed along the x axis (see Fig. 1). Though the HMS is in some respects similar to the widely studied diluted magnetic structures, it possesses some important advantages and differences that make the HMS not only a more feasible system to produce and to

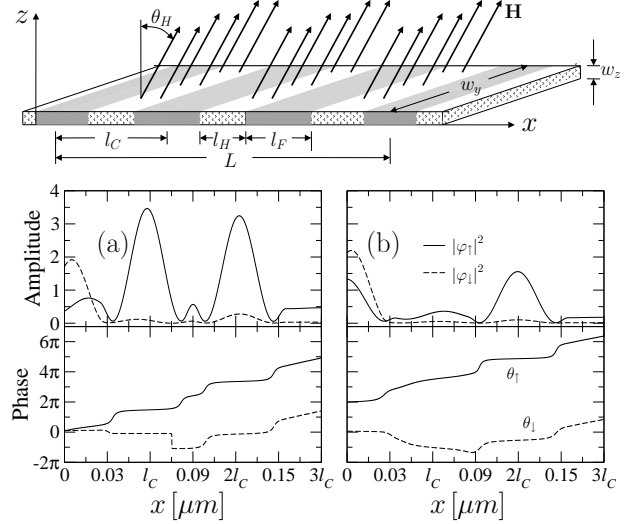


FIG. 1: A 3D semiconductor wave guide where an external homogeneous magnetic field \mathbf{H} is screened on alternating stripes of length l_F . The external magnetic field (tilted θ_H with respect to z), acts on the stripes of length l_H . We work in the quasi-2DEG limit: $w_z \ll w_y$. In the lower part, the wave-function amplitudes and phases for two specific values of H are shown. In (a) $T_{\uparrow,\uparrow} \simeq 0.87$, $R_{\uparrow,\uparrow} \simeq 0.005$, and $T_{\uparrow,\downarrow} \simeq 0.06$. The amplitude $|\varphi_{\downarrow}|^2$ follows $|\varphi_{\uparrow}|^2$ and both are practically in phase for $x \geq l_C/2$. In (b) $T_{\uparrow,\uparrow} \simeq 0.34$, $R_{\uparrow,\uparrow} \simeq 0.62$ but $T_{\uparrow,\downarrow} \simeq 0.024$. Thus, φ_{\downarrow} features remain deeper in the SL.

study theoretically, but also a system where the injection of electrons to and from the device is simpler. It is worth mentioning however that some basic quantities like the magnetic field strength H , the energy levels separation $\Delta E_{\nu\nu'}$, the subbands separation (related in some way to the operational temperatures T) and the geometrical parameters are crucially intertwined. Our calculations for InSb semiconductors (characterized by a large Landé g -factor and Dresselhaus coefficient $\beta_D \simeq 2.3eVnm^3$) suggest that for $L_H \sim 10nm$ and external magnetic fields of the order of 0.25T we can expect subbands separation of 15meV. To increase the subband separation, we need to

increase H and to reduce L_H . Increasing the subbands separation the operational temperature T increases. It is important to stress that the Schrödinger equation of this system containing a spin-orbit interaction is soluble. Hence, the spin dynamics is almost fully described. In our approach¹⁴ the wave function inside the device subject to external fields can be written as

$$\begin{pmatrix} \varphi_{\uparrow}(x) \\ \varphi_{\downarrow}(x) \end{pmatrix} = [(\alpha(x) + \gamma(x)) + \mathbf{r}_n(\beta(x) + \delta(x))] \begin{pmatrix} a_{\uparrow} \\ a_{\downarrow} \end{pmatrix}, \quad (1)$$

with a_{\uparrow} and a_{\downarrow} the incoming amplitudes, \mathbf{r} the reflection amplitude

$$\mathbf{r} = \begin{pmatrix} r_{\uparrow,\uparrow} & r_{\uparrow,\downarrow} \\ r_{\downarrow,\uparrow} & r_{\downarrow,\downarrow} \end{pmatrix}. \quad (2)$$

and $\alpha(x)$, $\beta(x)$, $\gamma(x)$ and $\delta(x)$ elements of a transfer matrix $M(x, 0)$ relating the incoming wave vector at the left of the device with the wave vector at x .

To calculate the device scattering amplitudes \mathbf{r} and \mathbf{t} , we use the theory of finite periodic system¹⁷. The transmission coefficient from channel j on the left to channel i on the right is given by $T_{i,j} = (\mathbf{t}\mathbf{t}^{\dagger})_{i,j}$. In our multi-mode approach we can also calculate the conductance and the resonant energies and wave functions, among other physical quantities. Knowing these quantities as functions of the field strength H , the tilting angle θ_H and the geometrical parameters, we can search for HMS's with the desired property. In the *absence of spin-mixing* (when $\beta_D = 0$ and $\theta_H = 0$) \mathbf{r} and \mathbf{t} are diagonal.

As mentioned before, clear signatures of coherent spin flipping processes can be inferred from the carrier's wave function behavior. To help visualizing part of the rich phenomenology emerging from our results, we show in the lower part of Fig. 1 the evolution of spin \uparrow and spin \downarrow wave-function amplitudes (WFA's) and phases, through a simple 3-cells magnetic superlattice (SL), for two specific cases differing only in the field strength H . Though the incoming electron beams in (a) and (b) are equally unpolarized, the WFA's inside the SL's are different. In (a) $T_{\uparrow,\uparrow}$ is large ($\simeq 0.87$) with low reflection ($R_{\uparrow,\uparrow} \simeq 0.005$), while $T_{\downarrow,\downarrow}$ is small ($= 0.006$) with high reflection ($R_{\downarrow,\downarrow} \simeq 0.87$). Because of these and the relatively large *transition coefficient* $T_{\uparrow,\downarrow} \simeq 0.06$, the amplitude $|\varphi_{\downarrow}|^2$ inside the SL follows the behavior of $|\varphi_{\uparrow}|^2$ and both functions are practically in phase after the first cell. This means that beyond the first cell the spin \downarrow electrons come basically from the spin \uparrow beam via spin inversion. In (b) $T_{\downarrow,\downarrow}$ and $R_{\downarrow,\downarrow}$ are almost the same as in (a) (0.003 and 0.95), while $T_{\uparrow,\downarrow}$ and $T_{\downarrow,\uparrow}$ are smaller (0.024 and 0.34) but $R_{\uparrow,\uparrow}$ is larger (0.62). Thus, the wave function φ_{\downarrow} features remain deeper (up to the second cell) in the SL.

In Ref¹⁶ the band structure of the transmission coefficients $T_{\uparrow,\uparrow}$, $T_{\uparrow,\downarrow}$ and $T_{\downarrow,\downarrow}$ were studied as functions of energy and θ_H . It was shown that increasing θ_H , the band structure of $T_{\uparrow,\uparrow}$ shifts towards lower energies while that of $T_{\downarrow,\downarrow}$ towards higher energies. On the other hand, it was

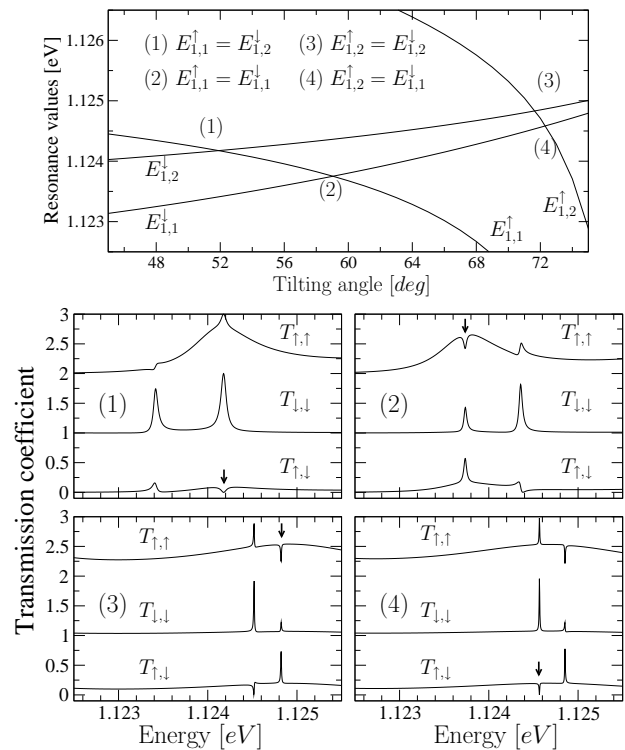


FIG. 2: In the top panel, the evolution of the resonant energies $E_{\mu\nu}^{\uparrow}$ and $E_{\mu\nu}^{\downarrow}$ as functions of the tilting angle θ_H is shown. In the bottom panels, we plot the transmission coefficients for each tilting angle where the resonant energies $E_{\mu\nu}^{\uparrow}$ and $E_{\mu\nu}^{\downarrow}$ cross. Fano anti-resonances appear in $T_{\uparrow,\uparrow}$ (with resonant $T_{\uparrow,\downarrow}$) when $\nu_{\uparrow} + \nu_{\downarrow} + n$ is odd (panels (2) and (3)). Fano line-shapes in $T_{\uparrow,\uparrow}$ with vanishing $T_{\uparrow,\downarrow}$ antiresonance appear when the previous sum is even (panels (1) and (4)).

also shown¹⁴ that growing H the transmission coefficient $T_{\uparrow,\uparrow}$ experiences a red shift, while $T_{\downarrow,\downarrow}$ a blue shift. In figure 2 we show energy levels and transmission coefficients of a three cell superlattice subject to $\mathbf{H} = H(0, \tan \theta_H, 1)$. In the upper part of this figure we show the evolution of energy levels as functions of θ_H . Here $E_{\mu,\nu}^i$ refers to the ν -th resonance in the μ -th subband, and i denotes the spin component. In the lower part, we plot the transmission coefficients for each crossing. In this figures the Fano-like antiresonances are pointed out with arrows. We found that $T_{\downarrow,\uparrow}$ antiresonances occur when $\nu_{\uparrow} + \nu_{\downarrow} + n$ is even, while $T_{\uparrow,\uparrow}$ antiresonances occur when the previous sum is odd¹⁹. Based on these selection rules and the band shift induced by the magnetic field, we propose a two-step spin inversion device consisting of two HMS's. The first SL is devoted to invert the largest fraction of the incoming spin \downarrow electrons, while the second SL filters the remaining spin \downarrow flux, to have only spin \uparrow electrons ($|\varphi_{\downarrow}(2L)|^2 = 0$) at the right of the device.

The behavior of the transmission coefficients at the resonance and antiresonance energies provides a clear insight on the effects and physical conditions required for the expected device performance. In panels (1) and (4)

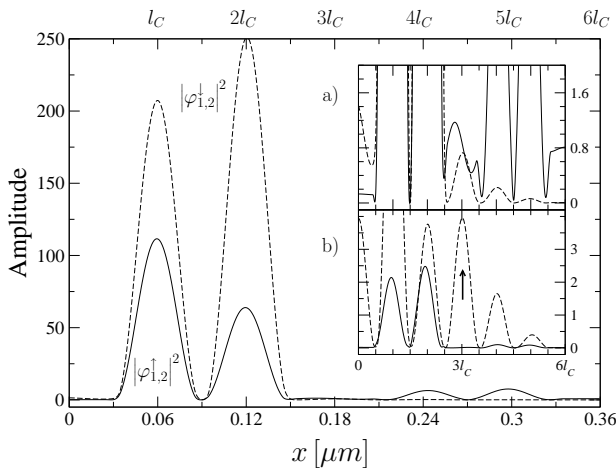


FIG. 3: Spin-up $|\varphi_{\uparrow}|^2$ and spin-down $|\varphi_{\downarrow}|^2$ wave functions in a two step inversion process. For a polarized spin \downarrow beam and high $T_{\uparrow,\downarrow}$ ($\sim 80\%$), the incoming plus the reflected wave function are mainly spin \uparrow at the left, while at the right hand side of the first SL the spin \uparrow flux is higher, with almost null spin \downarrow flux. To visualize better the spin \uparrow and \downarrow electrons distribution with energies 1.1248meV and 1.1245meV, we amplify these functions in the insets a) and b), respectively.

of Fig. 2 the transition probabilities $T_{\downarrow,\uparrow}$ and $T_{\uparrow,\downarrow}$ vanish at the resonance, while $T_{\uparrow,\uparrow}$ and $T_{\downarrow,\downarrow}$ are practically 1. Under these conditions, the system can neither filter nor polarize spin fluxes. On the other hand, the anti-resonances of $T_{\uparrow,\uparrow}$ shown in panels (2) and (3) lead to maximum transition probabilities ($T_{\uparrow,\downarrow}$ and $T_{\downarrow,\uparrow}$) along with a significant reduction of $T_{\downarrow,\downarrow}$. In these cases one

can figure out the possibility of designing a spin-polarizer or a spin-inversor device. In the particular example discussed here, the parameters of the three-cells SLs are: $l_F = w_y = 5.0 \times 10^{-2} \mu m$ and $l_H = 1.0 \times 10^{-2} \mu m$. In the first-step SL we choose $H = 200$ mT with $\theta_H = 71.44^\circ$ (the crossing angle of $E_{1,2}^{\uparrow}$ and $E_{1,2}^{\downarrow}$). In this case, the transition coefficient $T_{\uparrow,\downarrow} \simeq 0.77$. In the second step we have to filter the remaining spin \downarrow . In this SL $\theta_H = 0$ and $H = 250$ mT. As mention before, we can visualize the device performance in terms of the carriers probability distributions $|\varphi_{\nu\nu'}^{\uparrow}(x)|^2$ and $|\varphi_{\nu\nu'}^{\downarrow}(x)|^2$. In Fig. 3 we plot the spin wave eigenfunctions for $E_{1,2}^{\uparrow} = E_{1,2}^{\downarrow}$ all along the device. At the left of the first superlattice the incoming flux is fully spin \downarrow polarized. At the end of this superlattice, the population of spin \uparrow electrons increases proportionally to $T_{\uparrow,\downarrow}$, up to $\sim 80\%$. The second step SL is just a filter. Because of the Dresselhaus interaction a small fraction of the remaining spin \downarrow electrons become spin \uparrow (see inset a)). As can be seen in Fig.2, only spin \uparrow particles reach the right hand side of our device. The high transmission of spin \downarrow at 1.1245meV has negligible effect (as shown in the inset b)), because the spin filter operation-energy window is 15meV.

We have applied here the magnetic superlattice theory¹⁴ for designing a device that, using conveniently the Fano anti-resonance selection rules, changes the spin projection of almost the whole incident beam. Adding the second step the flux of the outgoing particles becomes fully polarized.

We acknowledge A. Robledo-Matínez, J. Grabinsky, M. Ruggero and M.-W. Wu for useful comments.

¹ I. Žutić, J. Fabian, and S. Das Sharma, Rev. Mod. Phys. **76**, 323 (2004).
² P. R. Hammar, B. R. Bennet, M. J. Yang and M. Johnson, J. Appl. Phys. **87**, 4665 (2000).
³ G. Prinz, Physics Today **48**, 58 (1995).
⁴ R. Fiederling, M. Keim, G. Reuscher, W. Ossau, G. Schmidt, A. Waag and L. W. Molenkamp, Nature **402**, 787 (1999).
⁵ Y. Ohno, D. K. Young, B. Beschoten, F. Matsukura, H. Ohno and D. D. Awschalom, Nature **402**, 790 (1999).
⁶ T. Koga, J. Nitta, H. Takayanagi and S. Datta, Phys. Rev. Lett. **88**, 126601 (2002).
⁷ M. Kohda, Y. Ohno, K. Takamura, F. Matsukura and H. Ohno, Jpn. J. Appl. Phys., Part 1, **40**, L1274 (2001).
⁸ E. Johnston-Halperin, D. Lofgreen, R. Kawakami, D. Young, L. Coldren, A. Gossard and D. Awschalom, Phys. Rev. B **65**, 041306 (2002).
⁹ Y. Kato, R. C. Myers, D. C. Driscoll, Gossard, J. Levy and D. D. Awschalom, Science **299**, 1201 (2003).
¹⁰ J. M. Kikkawa, I. P. Smorchkova, N. Samarth and D. D.

Awschalom, Science **277**, 1284 (1997).
¹¹ J. M. Kikkawa and D. D. Awschalom, Nature **1999**, 139 (397).
¹² J. F. Song, Y. Ochiai and J. P. Bird, Appl. Phys. Lett. **82**, 4561 (2003).
¹³ M. E. Torio, K. Hallberg, S. Flach, A. E. Miroshnichenko and M. Titov, Eur. Phys. J. B **37**, 399 (2004).
¹⁴ J. L. Cardoso, P. Pereyra and A. Anzaldo-Meneses, Phys. Rev. B **63**, 153301 (2001).
¹⁵ M. W. Wu, J. Zhou and Q. W. Shi, Appl. Phys. Lett. **85**, 1012 (2004).
¹⁶ P. Pereyra and J. L. Cardoso, Phys. Stat. Sol. (c) **4**, 462 (2007).
¹⁷ P. Pereyra, Phys. Rev. Lett. **80**, 2677 (1998).
¹⁸ We assume that a partial or total screening of the magnetic field is possible using μ -metals, superconductor paintings, etc.
¹⁹ A detailed analysis of these selection rules will be published elsewhere